

## Structure of the San Andreas fault zone at SAFOD from a seismic refraction survey

J. A. Hole,<sup>1</sup> T. Ryberg,<sup>2</sup> G. S. Fuis,<sup>3</sup> F. Bleibinhaus,<sup>1,4</sup> and A. K. Sharma<sup>1</sup>

Received 10 November 2005; revised 13 February 2006; accepted 6 March 2006; published 11 April 2006.

[1] Refraction traveltimes from a 46-km long seismic survey across the San Andreas Fault were inverted to obtain two-dimensional velocity structure of the upper crust near the SAFOD drilling project. The model contains strong vertical and lateral velocity variations from  $<2$  km/s to  $\sim 6$  km/s. The Salinian terrane west of the San Andreas Fault has much higher velocity than the Franciscan terrane east of the fault. Salinian basement deepens from 0.8 km subsurface at SAFOD to  $\sim 2.5$  km subsurface 20 km to the southwest. A strong reflection and subtle velocity contrast suggest a steeply dipping fault separating the Franciscan terrane from the Great Valley Sequence. A low-velocity wedge of Cenozoic sedimentary rocks lies immediately southwest of the San Andreas Fault. This body is bounded by a steep fault just northeast of SAFOD and approaches the depth of the shallowest earthquakes. Multiple active and inactive fault strands complicate structure near SAFOD. **Citation:** Hole, J. A., T. Ryberg, G. S. Fuis, F. Bleibinhaus, and A. K. Sharma (2006), Structure of the San Andreas fault zone at SAFOD from a seismic refraction survey, *Geophys. Res. Lett.*, *33*, L07312, doi:10.1029/2005GL025194.

### 1. Introduction

[2] As part of EarthScope ([www.earthscope.org](http://www.earthscope.org)), the San Andreas Fault Observatory at Depth (SAFOD) will drill into the source region of a repeating magnitude-2 earthquake on the San Andreas Fault (SAF) near Parkfield, California [Hickman *et al.*, 2004]. Detailed characterization of the subsurface geology and faulting surrounding the SAFOD site and SAF target is required to plan drilling and to interpret the down-hole results. Preliminary site characterization is summarized by Hickman *et al.* [2004].

[3] This paper presents a seismic P-wave velocity model derived from a 46-km-long refraction and reflection survey across the fault at the SAFOD site. The survey was designed to produce ray coverage and a subsurface velocity model to deeper than the drilling target. The model is interpreted in terms of regional geology and structure of the fault zone.

### 2. Data Acquisition and Analysis

[4] The data were acquired in November 2003 by an industry crew. The line was perpendicular to the SAF,

centered on the SAFOD drill site, and extended from the Salinas River north of Paso Robles to Coalinga (Figure 1). The line was deployed straight across country, assisted by helicopters, radio telemetry, and minor line clearing. A fixed array of 912 three-component MEMS (micro-electro-mechanical systems) digital accelerometers (flat response above 1.5 Hz) was deployed at 50-m spacing along the line, with 25-m spacing used for 5 km at the SAF. The line had two gaps due to lack of landowner permission. Sixty-three explosive sources were fired in boreholes along the line. An additional 5 shots were fired off the line near SAFOD but are not used here. The shot size was 100 kg at a nominal 1-km spacing along the entire line and 25 kg at a nominal 0.5-km spacing within 10 km of the SAF. Larger 200-kg shots were used at the ends of the line. Substantial relief and variation in near-surface conditions affected source and receiver coupling and produced large time shifts. A sample shot record near the SAF is shown in Figure 2.

[5] Several groups piggybacked on the refraction/reflection survey by recording the shots. These included: an array in the vertical SAFOD pilot hole; high-resolution surface arrays near SAFOD, the SAF, and Buzzard Canyon Fault (BCF; Figure 1); and temporary and permanent earthquake arrays.

[6] First-arrival travel times were picked for inline shots and receivers and inverted for two-dimensional seismic velocity structure. Both picking and tomographic inversion were performed independently at two institutions to test robustness of the analysis. Comparison of travel times picked by the two groups, shot-to-shot consistency, and shot-to-receiver-to-shot reciprocity indicated an accuracy of  $\sim 10$  ms at  $<10$  km shot-receiver offset degrading to  $\sim 100$  ms at  $>35$  km offset. Figure 3 shows the two velocity models.

[7] Figure 3a was derived using the algorithm of Hole [1992] and emphasizes a minimum-structure approach. The algorithm computes travel times through a finite-difference solution of the eikonal equation and inverts for velocity structure using back-projection. The grid spacing is 50 m. The starting model contained a linear increase in velocity with depth. Early iterations used extreme smoothing so that they provided for subsequent iterations a smooth starting model based upon the data. Slow convergence with gradually decreasing smoothing reduces dependence upon the starting model and produces a final model with minimal structure. Experimentation with different starting models, smoothing aspect ratios, and rates of decreasing smoothing size produced the preferred model shown. This model maximizes spatial resolution while minimizing artifacts such as streaks along dominant ray directions.

[8] Figure 3b was derived using the algorithm of Zelt and Barton [1998] and attempts to provide better spatial reso-

<sup>1</sup>Department of Geosciences, Virginia Polytechnic Institute and State University, Blacksburg, Virginia, USA.

<sup>2</sup>GeoForschungsZentrum, Potsdam, Germany.

<sup>3</sup>U.S. Geological Survey, Menlo Park, California, USA.

<sup>4</sup>Now at Department of Earth and Environmental Sciences, University of Munich, Munich, Germany.

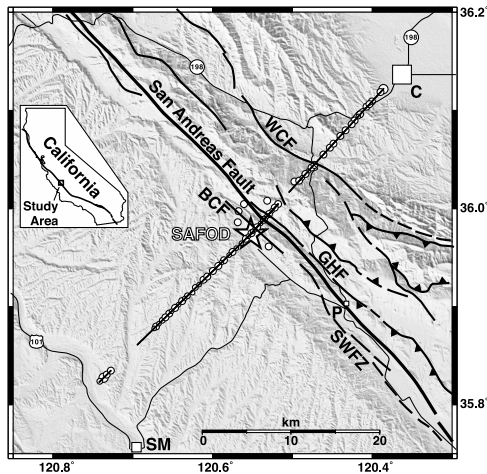


**Figure 1.** Map of SAFOD site (star) and 2003 seismic survey in central California. White circles are shots; coincident black line is receivers. Major faults (BCF, Buzzard Canyon; GHF, Gold Hill; SWFZ, Southwest Fracture Zone; WCF, Waltham Canyon) [from Jennings, 1977; Dibblee, 1971; Hole et al., 2001] are overlain on shaded-relief topography. Towns (C, Coalinga; SM, San Miguel; P, Parkfield) and major roads are shown.

lution at shallow depth. The algorithm computes travel times in the same manner as Hole [1992] but inverts the system of equations through conjugate gradients. The inversion grid spacing started at  $1.6 \times 0.8$  km to reduce dependence on the starting model, and was gradually reduced to  $100 \times 50$  m. Experimentation with different starting models, grid spacings, and smoothing produced the preferred model shown.

[9] Despite independent travel-time picks, inversion algorithms, and inversion strategies, the two velocity models show similar structures. Figure 3a is smoother. Figure 3b constrains higher-resolution near-surface structure, but has high-frequency artifacts in deeper parts of the model. The models have similar travel time misfits (root-mean-square 40–42 ms). Checkerboard tests and the experimentation described above indicate that resolution decreases from  $\sim 0.2$  km at sea level to  $\sim 0.5$  km at 2 km below sea level (bsl). Ray coverage and resolution deteriorate at  $>3$  km bsl due to decreasing velocity gradient with depth and limited picks at larger offsets.

### 3. Interpretation and Discussion

[10] Figure 3 shows strong lateral and vertical velocity variations that correspond to the major geologic units in the region (e.g., review given by Page et al. [1998]). A simple interpretation is shown in Figure 3c.

[11] Southwest of the SAF, low velocity (1.5–3.5 km/s) at shallow depth corresponds to late Cenozoic sedimentary rocks. A sharp velocity increase from  $<4$  to  $>5$  km/s marks the top of Mesozoic granitic and metamorphic rocks of the Salinian terrane (Figure 3c). The top of Salinian basement is at 0.77 km subsurface ( $\sim 0.1$  km bsl) in the SAFOD drill hole [Hickman et al., 2004], as predicted by higher-resolution seismic studies [Hole et al., 2001; Catchings et al., 2002]. Basement velocity is consistent with the 5 to 5.65 km/s

observed in the pilot hole [Boness and Zoback, 2004]. The basement – cover contact deepens to the southwest, to  $\sim 2$  km bsl at the southwest end of the line (Figure 3c). Sharp offsets in the velocity contours suggest faults offsetting basement.

[12] Seismic velocity is much lower northeast of the SAF (Figure 3), corresponding to mostly sedimentary accretionary wedge rocks of the Mesozoic Franciscan terrane. Velocity of  $<5$  km/s persists to  $>4$  km bsl. Further northeast, the Waltham Canyon Fault (WCF) (Figure 1) separates the Franciscan terrane from folded sedimentary rocks of the Cretaceous to Tertiary Great Valley Sequence. The WCF dips to the southwest and it locally splays eastward relative to the regional trend of the terrane-bounding Coast Range Fault [Jennings, 1977; Dibblee, 1971]. The velocity contrast is subtle across this terrane boundary (Figure 3). Strong reflections observed in shot gathers have been migrated to image a near-vertical reflector  $\sim 1.5$  km southwest of the WCF [Bleibinhaus et al., 2005], roughly beneath the regional trend of the terrane boundary. The reflector (solid red line in Figure 3c) and WCF (dashed red line) are interpreted as reverse faults bounding the Franciscan terrane and Great Valley Sequence.

[13] Near the SAF and SAFOD, high velocity granitic rocks of the Salinian terrane do not extend to the surface trace of the SAF above  $\sim 3$  km bsl (Figure 3). The location of the top and edge of granitic rock was tested by inversion for a refracting interface [Hole et al., 1992]. The near-horizontal top of Salinian basement ends abruptly 1.6 km southwest of the surface trace of the SAF (0.2 km northeast of SAFOD). The two velocity models shown in Figure 3 represent the least steep ( $\sim 45^\circ$ ) and steepest ( $\sim$ vertical) edge of granitic rock allowed by the data. At  $\sim 3$  km bsl, high-velocity basement extends closer to the surface trace of the SAF. Thus a steep wedge of low seismic velocity exists between Salinia and the SAF in the uppermost crust. The shallowest earthquakes are  $\sim 2$  km bsl [Thurber et al., 2004], at or near the base of this wedge.

[14] Shallow seismic refraction data first observed this low-velocity body [Hole et al., 2001; Catchings et al., 2002] but were limited to  $<1$  km depth. Three-dimensional earthquake tomography, incorporating data from explosions plus the shallow refraction data, extended the low velocity between SAFOD and the SAF to 1–3 km bsl [Thurber et al., 2003, 2004; Roecker et al., 2004]. Figure 3 is consistent with the earthquake tomography models but provides higher spatial resolution above 2–3 km bsl. This wedge of low

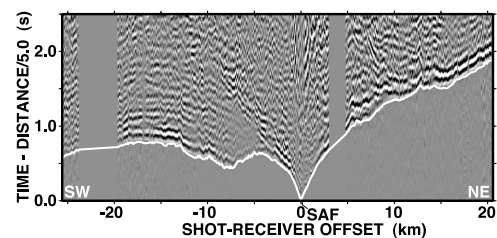


**Figure 2.** Seismic shot record for a small (25 kg) source located 0.2 km SW of the SAF. The time axis is reduced with a linear moveout of 5 km/s. Data are low-pass frequency filtered, edited for noisy traces, and trace normalized. Asymmetry across the SAF is strong. White line is travel times calculated in the model of Figure 3a.

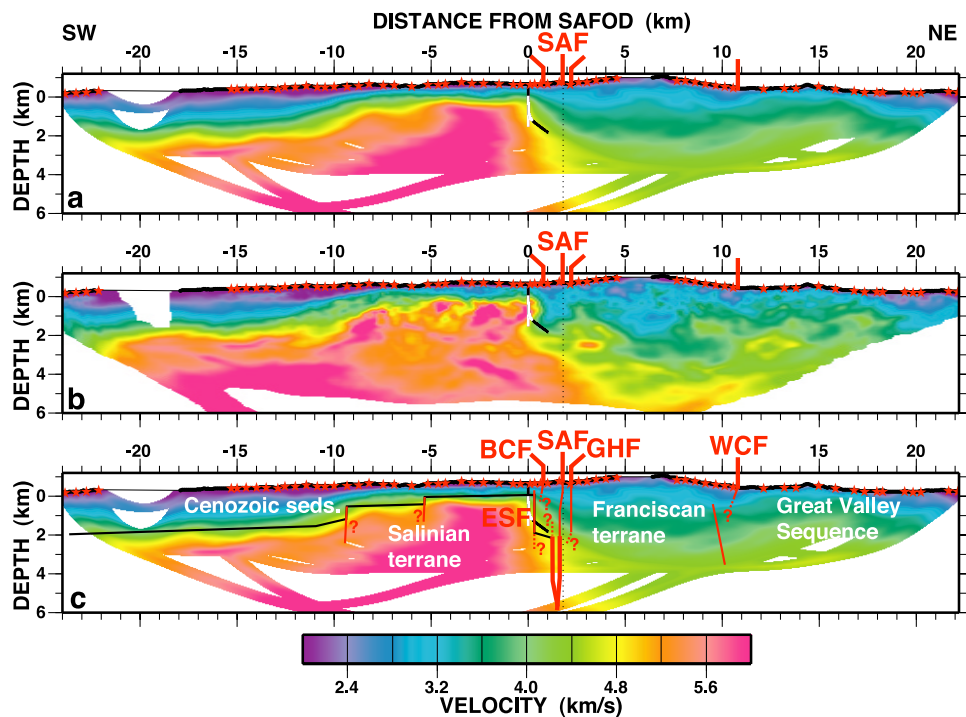


**Figure 3.** Seismic velocity model along the seismic line derived from first arrival traveltimes tomography. Shots are red stars and receivers are the thick black line. Regions without rays are white. Well-log observations at SAFOD are white for granite and black for sedimentary rock. (a) Minimum-structure model derived from 41,301 travel time picks using the algorithm of *Hole* [1992] and very slow convergence with large smoothing. (b) Model derived from 45,247 independent picks using the algorithm of *Zelt and Barton* [1998] and faster convergence with less smoothing. (c) Geology and fault interpretation overlaid on the model in Figure 3a. Black lines are top of Salinian basement; red lines are faults. Thicker faults at depth indicate seismicity.

velocity corresponds to a zone of high electrical conductivity [Unsworth *et al.*, 1997, 2000; Unsworth and Bedrosian, 2004]. Gravity data indicate that the body also has lower density than adjacent granitic rocks [McPhee *et al.*, 2004].

[15] Unsworth *et al.* [1997, 2000] and Unsworth and Bedrosian [2004] interpreted the high electrical conductivity as a broad fault zone containing extensive fracturing and saline fluids. *Hole et al.* [2001], *Catchings et al.* [2002], and *Park and Roberts* [2003] re-interpreted the coinciding low seismic velocity and high conductivity as a fault-bounded wedge of late Cenozoic sedimentary rocks. Drilling in 2004 encountered deep sedimentary rock between SAFOD and the SAF, drilling laterally from granite into sedimentary rock at 1.2 km bsl at 0.2 km northeast of SAFOD (Figure 3) [Hickman *et al.*, 2004]. The model of Figure 3b agrees remarkably well with the extent of granite in the borehole. The required conductive fluids correspond spatially to sedimentary rock and could be formation fluids and/or fault related.

#### 4. Fault Structure Near SAFOD

[16] Three major faults, the Gold Hill Fault (GHF), SAF, and BCF, are exposed at the surface near SAFOD (Figures 1 and 3c). An additional fault is constrained in the subsurface by imaging and drilling.

[17] The GHF is a moderately dipping (oblique?) thrust fault near Parkfield (Figure 1). It converges toward the SAF until it is  $\sim 0.3$  km northeast of the SAF at the seismic line.

There are no indications of recent activity. Figure 3b shows a lateral variation in velocity (blue to green) beneath the GHF at 0–1 km bsl. *Hole et al.* [2001] and *Bleibinhaus et al.* [2005] imaged strong vertical seismic reflectors directly beneath the surface trace of the GHF from 0.3 km above to  $\sim 2$  km bsl. These observations suggest that the GHF may be very steep at this location (Figure 3c).

[18] The surface trace of the SAF has obvious geomorphic indicators of activity, including an offset fence near the seismic line. Earthquakes occur below  $\sim 2.9$  km subsurface [Thurber *et al.*, 2004]. Seismicity defines a near vertical plane, but the deep fault may be offset one to several hundred meters to the southwest of the surface trace [Hole *et al.*, 2001; Thurber *et al.*, 2004]. Double-difference earthquake relative locations [Nadeau *et al.*, 2004; Waldhauser *et al.*, 2004] indicate two parallel strands of active seismicity 0.3 km apart that merge at  $>5$  km depth (indicated by thick red lines in Figure 3c). SAFOD drilling in 2005 observed multiple fault strands, at least two of which are active and hundreds of meters southwest of the surface SAF [Zoback *et al.*, 2005].

[19] The BCF (the then-unnamed fault “nF” of *Hole et al.* [2001]) is 1.0 km southwest of and parallel to the surface trace of the SAF (Figure 1). It is en echelon with the active Southwest Fracture Zone near Parkfield. The BCF dips steeply southwest and shows geomorphic evidence of recent activity (M. J. Rymer, personal communication, 2004).

[20] We interpret the presence of a fourth fault bounding the southwest edge of the deep body of Cenozoic sediments southwest of the SAF. Seismic velocity constrains sub-

horizontal basement to end 0.2 km northeast of SAFOD, and drilling intersected the edge of granite 1.2 km below this point [Hickman *et al.*, 2004]. We connect the two constrained points with a vertical fault (ESF in Figure 3c). No surface fault has been mapped at this location, suggesting that it is no longer active. The steep edge of high-velocity granitic rock steps to the northeast at the base of the sedimentary wedge (Figure 3). The edges and bottom of the high conductivity body of Unsworth *et al.* [1997, 2000] and Unsworth and Bedrosian [2004] can be interpreted in their smooth images as corresponding to the faulted edge of Salinia and either the SAF or GHF.

[21] The geometry of fault splays, intersections, and overlaps strongly influences the orientation of stress [e.g., Maerten *et al.*, 2002]. The structural relationships at depth between the GHF, SAF, BCF, faulted edge of Salinia, and two strands of active seismicity have not yet been imaged. Knowing the geometry of these faults and adjacent geologic units with different strengths is critical to interpreting stress observed in the SAFOD borehole [e.g., Scholz and Saucier, 1993], which is a primary goal of the project. Ongoing reflection, diffraction, and S-wave imaging from the 2003 seismic line, combined with geologic mapping and observations down hole, will improve the structural image.

[22] **Acknowledgments.** This work was funded by U.S. National Science Foundation grant EAR-0106534, the Deutsche Forschungsgemeinschaft, and the GeoForschungsZentrum Potsdam. Kinetex Inc. acquired the data. Acknowledgment is given to the landowners who provided access to private land. Steve Hickman aided in coordination of field logistics with landowners and with scientists who recorded our shots. Thanks go to the many people involved in the field work.

## References

- Bleibinhaus, F., J. A. Hole, and T. Ryberg (2005), Seismic reflection and diffraction imaging of the San Andreas Fault at SAFOD, *Eos Trans. AGU*, 86(47), Fall Meet. Suppl., Abstract T21A-0446.
- Boness, N. L., and M. D. Zoback (2004), Stress-induced seismic velocity anisotropy and physical properties in the SAFOD Pilot Hole in Parkfield, CA, *Geophys. Res. Lett.*, 31, L15S17, doi:10.1029/2003GL019020.
- Catchings, R. D., M. J. Rymer, M. R. Goldman, J. A. Hole, R. Huggins, and C. Lippus (2002), High resolution seismic velocities and shallow structure of the San Andreas fault zone at Middle Mountain, Parkfield, California, *Bull. Seismol. Soc. Am.*, 92, 2493–2503.
- Dibblee, T. W., Jr. (1971), Geologic maps of 17 15-minute quadrangles along the San Andreas Fault in the vicinity of King City, Coalinga, Panoche Valley, and Paso Robles, with index map, *U.S. Geol. Surv. Open File*, 71–87.
- Hickman, M., M. Zoback, and W. Ellsworth (2004), Introduction to special section: Preparing for the San Andreas Fault Observatory at Depth, *Geophys. Res. Lett.*, 31, L12S01, doi:10.1029/2004GL020688.
- Hole, J. A. (1992), Nonlinear high-resolution three-dimensional seismic travel time tomography, *J. Geophys. Res.*, 97, 6553–6562.
- Hole, J. A., R. M. Clowes, and R. M. Ellis (1992), Interface inversion using broadside seismic refraction data and three-dimensional travel time calculations, *J. Geophys. Res.*, 97, 3417–3429.
- Hole, J. A., R. D. Catchings, K. C. St. Clair, M. J. Rymer, D. A. Okaya, and B. J. Carney (2001), Steep-dip seismic imaging of the shallow San Andreas Fault near Parkfield, *Science*, 294, 1513–1515.
- Jennings, C. W. (1977), Geologic map of California, *Geol. Data Map 2*, scale 1:750,000, Calif. Div. of Mines and Geol., Sacramento.
- Maerten, L., P. Gillespie, and D. D. Pollard (2002), Effects of local stress perturbation on secondary fault development, *J. Struct. Geol.*, 24, 145–153.
- McPhee, D. K., R. C. Jachens, and C. M. Wentworth (2004), Crustal structure across the San Andreas Fault at the SAFOD site from potential field and geologic studies, *Geophys. Res. Lett.*, 31, L12S03, doi:10.1029/2003GL019363.
- Nadeau, R. M., A. Michelini, R. A. Uhrhammer, D. Dolenc, and T. V. McEvilly (2004), Detailed kinematics, structure and recurrence of microseismicity in the SAFOD target region, *Geophys. Res. Lett.*, 31, L12S08, doi:10.1029/2003GL019409.
- Page, B. M., G. A. Thompson, and R. G. Coleman (1998), Late Cenozoic tectonics of the central and southern Coast Ranges of California, *Geol. Soc. Am. Bull.*, 110, 846–876.
- Park, S. K., and J. J. Roberts (2003), Conductivity structure of the San Andreas Fault, Parkfield, revisited, *Geophys. Res. Lett.*, 30(16), 1842, doi:10.1029/2003GL017689.
- Roecker, S., C. Thurber, and D. McPhee (2004), Joint inversion of gravity and arrival time data from Parkfield: New constraints on structure and hypocenter locations from the SAFOD drill site, *Geophys. Res. Lett.*, 31, L12S04, doi:10.1029/2003GL019396.
- Scholz, C. H., and F. J. Saucier (1993), What do the Cajon Pass stress measurements say about stress on the San Andreas Fault? Comment on “In situ stress measurements to 3.5 km depth in the Cajon Pass scientific research borehole: Implications for the mechanics of crustal faulting” by Mark D. Zoback and John H. Healy, *J. Geophys. Res.*, 98, 17,867–17,870.
- Thurber, C., S. Roecker, K. Roberts, M. Gold, L. Powell, and K. Rittger (2003), Earthquake locations and three-dimensional fault zone structure along the creeping section of the San Andreas Fault near Parkfield, CA: Preparing for SAFOD, *Geophys. Res. Lett.*, 30(3), 1112, doi:10.1029/2002GL016004.
- Thurber, C., S. Roecker, H. Zhang, S. Baher, and W. Ellsworth (2004), Fine-scale structure of the San Andreas fault zone and location of the SAFOD target earthquakes, *Geophys. Res. Lett.*, 31, L12S02, doi:10.1029/2003GL019398.
- Unsworth, M., and P. A. Bedrosian (2004), Electrical resistivity structure at the SAFOD site from magnetotelluric exploration, *Geophys. Res. Lett.*, 31, L12S05, doi:10.1029/2003GL019405.
- Unsworth, M. J., P. E. Malin, G. D. Egbert, and J. R. Booker (1997), Internal structure of the San Andreas Fault at Parkfield, California, *Geology*, 25, 359–362.
- Unsworth, M. J., M. Eisel, G. D. Egbert, W. Siripunvaraporn, and P. A. Bedrosian (2000), Along-strike variations in the electrical structure of the San Andreas Fault at Parkfield, California, *Geophys. Res. Lett.*, 27, 3021–3024.
- Waldhauser, F., W. L. Ellsworth, D. P. Schaff, and A. Cole (2004), Streaks, multiplets and holes: High-resolution spatio-temporal behavior of Parkfield seismicity, *Geophys. Res. Lett.*, 31, L18608, doi:10.1029/2004GL020649.
- Zelt, C. A., and P. J. Barton (1998), 3D seismic refraction tomography: A comparison of two methods applied to data from the Faeroe Basin, *J. Geophys. Res.*, 103, 7187–7210.
- Zoback, M. D., S. Hickman, and W. Ellsworth (2005), Overview of SAFOD phases 1 and 2: Drilling, sampling, and measurements in the San Andreas fault zone at seismogenic depth, *Eos Trans. AGU*, 86(47), Fall Meet. Suppl., Abstract T23E-01.

F. Bleibinhaus, Department of Earth and Environmental Sciences, University of Munich, Theresienstr. 41, D-80333 Munich, Germany. (bleibi@geophysik.uni-muenchen.de)

G. S. Fuis, U. S. Geological Survey, 345 Middlefield Rd., MS977, Menlo Park, CA 94025, USA. (fuis@usgs.gov)

J. A. Hole and A. K. Sharma, Department of Geosciences, Virginia Tech, 4044 Derring Hall, Blacksburg, VA 24061, USA. (hole@vt.edu; arsharma@vt.edu)

T. Ryberg, GeoForschungsZentrum, Telegrafenberg E322, D-14471 Potsdam, Germany. (trond@gfz-potsdam.de)